

Structural and Electrical Studies of Aluminium-doped Nickel-Cobalt Ferrite Nanoparticles

S. P. Waghmare^a, D. M. Borikar^a, M. A. Borikar^b and K. G. Rewatkar^c

^aDepartment of Chemistry, Dr. Ambedkar College, Deekshabhoomi, Nagpur, India.

^bDepartment of Chemistry, St. Vincent Palloti College of Engg. & Tech., Nagpur, India.

^cDepartment of Physics, Dr. Ambedkar College, Deekshabhoomi, Nagpur, India.

Doi: <https://doi.org/10.47011/15.1.4>

Received on: 01/08/2020;

Accepted on: 29/6/2021

Abstract: Aluminium-doped Nickel-Cobalt ferrite nanoparticles with general formula $\text{Ni}_{0.5}\text{Co}_{0.5}\text{Al}_x\text{Fe}_{2-x}\text{O}_4$ ($x = 0$ and $x = 0.5$) were synthesized by microwave-assisted sol-gel auto-combustion method. The X-ray diffraction analysis of the samples confirms single phase with cubic spinel structure belonging to space group Fd3m. The average crystallite size calculated using Debye-Scherrer formula was found to be in the range of 19-36 nm. XRD studies revealed that the lattice parameter (a), the particle size (D) and X-ray density (d_x) decrease, whereas porosity increases with Al substitution. Energy Dispersive X-ray (EDX) was used to confirm the elemental composition of synthesized powders. TEM micrograph suggests that the particle size is in nanometric range, which confirms the nanocrystalline nature of the samples. The electrical resistivity and dielectric constant have been studied as functions of temperature. It was observed that the electrical resistivity decreases with increasing temperature, exhibiting the semiconducting nature of the sample. The dielectric constant increases with increase in temperature up to transition temperature and then decreases, which is explained on the basis of hopping mechanism.

Keywords: Ni-Co ferrites, Sol-Gel, XRD, Resistivity, Dielectric constant.

Introduction

Nanostructured spinel ferrites play an important role in the technological applications because of their interesting chemical stability, electric and dielectric properties [1]. Recent research reports that mixed nanoferrites usually have better performance than conventional nanoferrites and nanospinel ferrite nickel-cobalt ferrites are of technical importance due to their unique electrical and dielectric properties. They have been used for numerous applications, including microwave devices, gas sensors, magnetic fluids, recording media, ferro-fluids, high-density information storage and catalysis [2]. The general chemical formula of spinel ferrites is MFe_2O_4 , where M is the divalent metal cation. The spinel ferrite structure consists of

close-packed oxygen arrangement in which tetrahedral (A) sites and octahedral (B) sites are occupied by the cation [3]. This structure allows incorporation of different metallic ions without altering the basic crystal structure of spinel ferrites [4]. Substitution of non-magnetic ions in spinel ferrites was found to alter their electric and magnetic properties [5]. Al^{3+} -substituted nickel-cobalt ferrite shows high stability and high electrical resistivity [6]. Such materials can be used in data-storage devices [7]. To our best knowledge, structural and electrical properties of aluminium-substituted nickel-cobalt ferrite were not documented yet. By keeping this fact into consideration, we have chosen Al-substituted nickel-cobalt ferrite to study these properties.

Many methods have been reported for the synthesis of spinel nanoferrites. Among the several methods, microwave-assisted Sol-Gel auto-combustion method is primarily selected because of many advantages, such as rapid heating, shorter processing time, fast reaction, efficient energy transformation and volume heating, high purity, high yield, easy reproducibility, particle size and shape control, homogeneity and improved characteristics [8].

In the present work, we have reported the synthesis of nickel-cobalt ferrite with aluminium substitution using microwave-assisted sol-gel auto-combustion method and investigation of their structural, electrical and dielectric properties.

Experimental

Synthesis Technique

Nano-crystalline powders of $\text{Ni}_{0.5}\text{Co}_{0.5}\text{Al}_x\text{Fe}_{2-x}\text{O}_4$ ($x = 0$ and $x = 0.5$) have been synthesized *via* microwave-assisted sol-gel auto-combustion method. The stoichiometric amounts of AR grade nickel nitrate $\text{Ni}(\text{NO}_3)_2 \cdot 6\text{H}_2\text{O}$, cobalt nitrate $\text{Co}(\text{NO}_3)_2 \cdot 6\text{H}_2\text{O}$, iron nitrate $\text{Fe}(\text{NO}_3)_3 \cdot 9\text{H}_2\text{O}$ and aluminium nitrate $\text{Al}(\text{NO}_3)_3 \cdot 9\text{H}_2\text{O}$ were used, while urea $\text{Co}(\text{NH}_2)_2$ was used as fuel. The mixture of metal nitrate and urea was dissolved in minimum quantity of distilled water. Condensation reaction occurs between the adjoining metal nitrates and urea, yielding a polymer network in colloidal dimensions known as 'sol'.

The beaker containing 'sol' is continuously stirred using a hot-plate magnetic stirrer and constantly maintained at temperatures of 70°C - 80°C in order to evaporate water in excess. The resulting viscous liquid foams ignite and undergoes a self-sustained combustion, producing 'gel' by slow drying process. Further, the wet gel is fired in a specially designed microwave oven, to get the resultant ash powder. The ashes of raw substances obtained were ground in a pestle and mortar for 4 hrs. Finally, these samples were annealed at 800°C for several hours at a heating rate of 100°C/hr so as to obtain single-phase nano-spinel ferrite.

X-ray Diffraction (XRD) Analysis

Structural analysis and phase identification of the synthesized samples were carried out by Philips X-ray diffractometer (Model 3710) using

$\text{CuK}\alpha$ radiation of wavelength $\lambda = 1.54 \text{ \AA}$ at room temperature. In this present research study, the expected sample structure is of spinel ferrite having cubic crystal lattice and therefore, the unit cell is characterized by the value of lattice parameter 'a', which is calculated from the equation:

$$a = [d^2 (h^2 + k^2 + l^2)]^{1/2} \quad (1)$$

where, d is the value of d -spacing of line in XRD pattern and h, k, l are the corresponding indices to each line in the XRD pattern.

The X-ray density (d_x) and bulk density (d_b) were also determined using the following formulae:

$$d_x = \frac{ZM}{N_A V} \quad (2)$$

$$d_b = \frac{m}{\pi r^2 h} \quad (3)$$

where, M is the molecular mass of the sample, Z is the number of formula units in a unit cell which is 8 for spinel ferrite, N_A is the Avogadro's number, V is the unit cell volume, m is the mass of the pellets, r is the radius of the pellets, h is the thickness of the pellet.

By comparing the X-ray density with bulk density, the % porosity (P) of the materials was calculated by using the equation:

$$P = 1 - \frac{d_x}{d_b} \times 100. \quad (4)$$

The average crystalline size of the samples was determined from the most intense peak (311) in the X-ray patterns using Debye-Scherrer's formula [9]:

$$D = \frac{K\lambda}{\beta \cos\theta} \quad (5)$$

where, λ is the wavelength of X rays which is equal to 1.54 \AA , K is the shape factor which is equal to ~ 0.9 for nano-spinel ferrites, β is the line broadening at the full width at half maximum (FWHM) intensity in radians.

Energy Dispersion X-ray (EDX) Spectroscopy

Elemental analysis has been conducted and chemical characterization of synthesized samples has been determined using energy dispersive X-ray spectroscopy EDX which was carried out by SEM-JSM-7600F operating at an accelerating voltage of 0.1 to 30 kV.

Transmission Electron Microscopy (TEM) Analysis

TEM analysis was carried out by the instrument of make PHILIPS, Model CM200, having an operating voltage of 20-200 kV and a resolution of 2.4 Å for nickel-cobalt ferrite nanoparticles.

Electric and Dielectric Measurements

For studying the electrical resistivity and dielectric constant of the samples, the samples were made in pellet form with a thin layer of silver pasted on both the flat faces to provide a better electrical contact and by applying a D.C. voltage across the pellet in four-probe Precision Impedance Analyzer 6500B Wayne Kerr at the frequency of 100 Hz. The measurements of electric resistivity (ρ) were carried out over the temperature range 250K-500K. The variation of dielectric constant (ϵ') was measured from 300K-800K.

Results and Discussion

XRD Analysis

The X-ray diffraction patterns of $\text{Ni}_{0.5}\text{Co}_{0.5}\text{Al}_x\text{Fe}_{2-x}\text{O}_4$ ($x = 0$ and $x = 0.5$) are shown in Fig.1. The XRD patterns were analyzed using X- Powder software and the crystalline phases were identified by comparison with reference data from the JCPDS card No.89-4927 for nickel ferrite and 22-1086 for cobalt ferrite. XRD pattern revealed the formation of single phased cubic spinel structure belonging to space group $\text{Fd}\bar{3}\text{m}$. Bragg's reflections were indexed which confirmed the formation of a well-defined single phase cubic structure without any trace of impurity. The diffraction peaks can be indexed for the Miller Indices (111), (220), (311), (400), (422), (511) and (440), which are all allowed peaks.

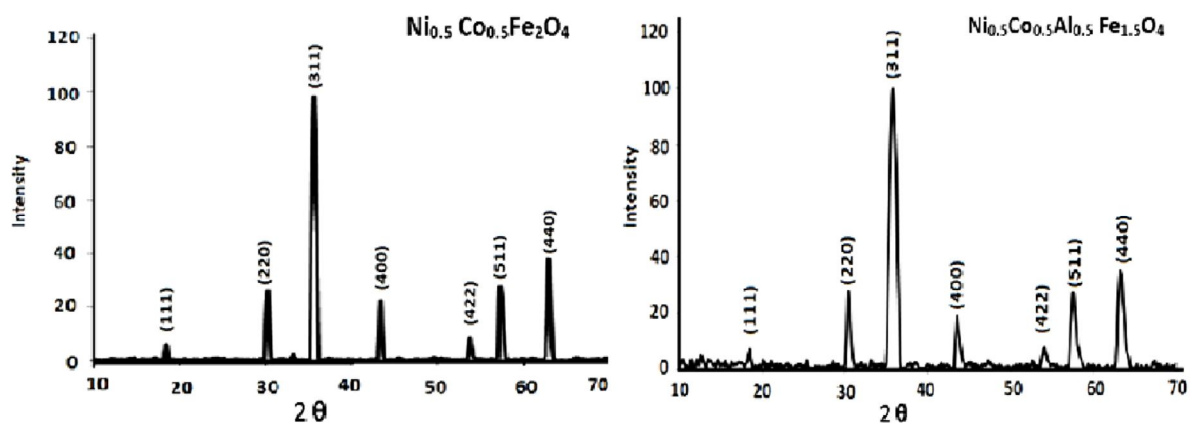


FIG. 1. X-ray diffraction pattern of $\text{Ni}_{0.5}\text{Co}_{0.5}\text{Al}_x\text{Fe}_{2-x}\text{O}_4$ ($x = 0$ and $x = 0.5$).

The particle size of the synthesized ferrite samples has been calculated from the most intense peak corresponding to (311) using the classical Debye-Scherrer formula. The values of lattice constant, X-ray density, bulk density, porosity and particle size were deduced from the X-ray data and are given in Table1. It is found that doping of Al^{3+} in the nickel-cobalt nanoferrite results in the decrease of lattice constant, which obeys the Vegard's law [10].

This decrease in lattice constant causes the XRD peaks to be shifted to the higher 2θ values, which can be clearly seen in Table1. The shifting of peaks towards higher angles and the decrease of lattice parameter 'a' show that Al atoms have been incorporated into the spinel structure of nickel-cobalt ferrite [11].

The peak intensities of (220) and (440) signals are more responsive to the cations in tetrahedral and octahedral sites, respectively [12, 13]. From Table 1, it is clearly seen that the intensity of (440) decreases with the addition of Al^{3+} ions, whereas the increase in intensity of (220) is due to migration of Fe^{3+} ions from octahedral site to tetrahedral site as Fe^{3+} ions are replaced by Al^{3+} ions [14]. This decreasing behavior of lattice constant is explained on the basis of difference in the ionic radii of Al^{3+} and Fe^{3+} . In the present study, larger Fe^{3+} ions having an ionic radius of 0.67 Å are replaced by smaller Al^{3+} ions having an ionic radius of 0.51 Å. Therefore, a decrease in lattice constant is observed which causes the shrinking of unit cell dimensions. Similar behavior of lattice constant was reported by A. Amirabadizadehet *al.* [15].

TABLE 1. X-ray diffraction parameters for the samples of $\text{Ni}_{0.5}\text{Co}_{0.5}\text{Al}_x\text{Fe}_{2-x}\text{O}_4$ ($x = 0$ and $x = 0.5$).

Sr. No.	Al content (x)	a (\AA) \pm 0.002	2θ (311) \pm 0.01	I (220)	I (440)	dx (gm/cm^3)	$d_b(\text{gm/cm}^3)$	P (%)	D (nm)
1	x = 0	8.352	35.64	26.7	22.0	5.347	2.4870	52.92	36
2	x = 0.5	8.311	35.81	27.9	18.8	5.147	2.3591	53.23	20

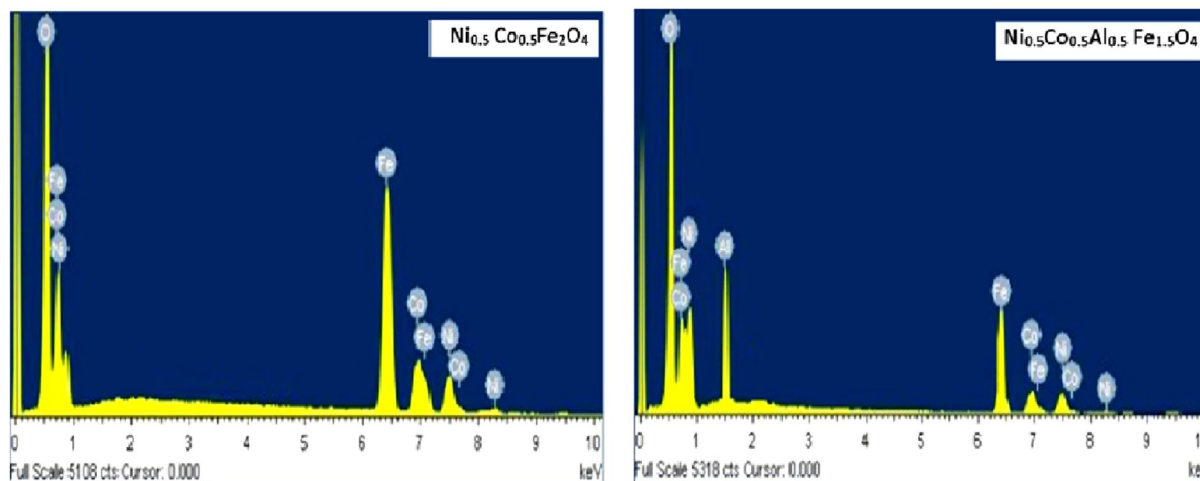
The X-ray densities and bulk densities are found to decrease with the addition of dopant Al^{3+} . This is due to replacement of heavier Fe^{3+} (55.85 amu) atoms by lighter Al^{3+} (26.98 amu) atoms [16]. From Table 1, it is also observed that x-ray densities of both samples are greater than the corresponding bulk densities due to the presence of pores in the synthesized sample [17].

The values of porosity of the synthesized sample are calculated using x-ray densities and bulk densities. From Table 1, it is observed that porosity of the samples increases with addition of aluminium. This may be due to the decrease in density with aluminium substitution and

evolution of gases like N_2 , H_2O and CO_2 during the combustion process favoring increased porosity. It has been found from Table 1 that the crystallite sizes are in the nanometer range of 19-36 nm and show a decrease with addition of aluminium. This observation resembles the reported results [15].

Energy Dispersion X-ray (EDX) Analysis

The EDX spectra of nickel-cobalt and aluminium-substituted nickel-cobalt ferrites are shown in Fig. 2. The weight percentage and atom percentage of different elements present in the samples are given in Table 2.

FIG. 2. EDX spectra of $\text{Ni}_{0.5}\text{Co}_{0.5}\text{Al}_x\text{Fe}_{2-x}\text{O}_4$ ($x = 0$ and $x = 0.5$).TABLE 2. Elemental composition of $\text{Ni}_{0.5}\text{Co}_{0.5}\text{Al}_x\text{Fe}_{2-x}\text{O}_4$ ($x = 0$ and $x = 0.5$).

Sr. No.	Al content(x)	Elements	Weight%	Atom%
1	x = 0	Ni	12.51	7.14
		Co	12.57	7.14
		Fe	47.63	28.55
		O	27.29	57.14
		Total	100.00	99.97
2	x = 0.5	Ni	13.34	7.14
		Co	13.39	7.14
		Al	6.13	7.14
		Fe	38.06	21.44
		O	29.08	57.15
Total	100.00	100.01		

From EDX plots and values given in Table 2, it is clear that there is no trace of impurity and no loss of any ingredient was found in the compounds. The characteristics peaks of Ni, Co, Fe, O and Al elements were observed in EDX spectra confirming the presence of all constituting elements in the prepared nano-spinel ferrite. EDX study also suggests that all the precursors have undergone a complete reaction to produce the nickel-cobalt and aluminium substituted nickel-cobalt spinel nanoferrites [18].

Transmission Electron Microscopy (TEM) Analysis

TEM was employed to confirm the details about the shape and size, microstructure, morphology and nanocrystalline nature of aluminium-substituted nickel-cobalt ferrite.

Fig. 3(a) shows the TEM micrograph of aluminium-substituted nickel-cobalt ferrite nanoparticles. It is clear from the figure that nanoparticles of synthesized aluminium-substituted nickel-cobalt ferrites are uniform in

morphology and crystalline size with some clustering/agglomeration between the particles.

The average particle size observed from the TEM micrographs is found to be in good agreement with the size calculated from the XRD analysis, confirming the formation of single-phase cubic structure.

The crystalline structure and detailed morphology of aluminium-substituted nickel-cobalt ferrite were further investigated by TEM bright-field images with corresponding Selected Area Electron Diffraction (SAED) patterns. SAED patterns of these samples are shown in Fig 3(b), which indicates that SAED pattern consists of well-defined spotted concentric rings, indicating the polycrystalline nature of synthesized nanoferrites. Similar observations have been reported by M. Lakshmi *et al.* [3].

The average particle size observed from the TEM micrograph is found to be in the range equal to that estimated from the XRD analysis, suggesting the formation of single crystals.

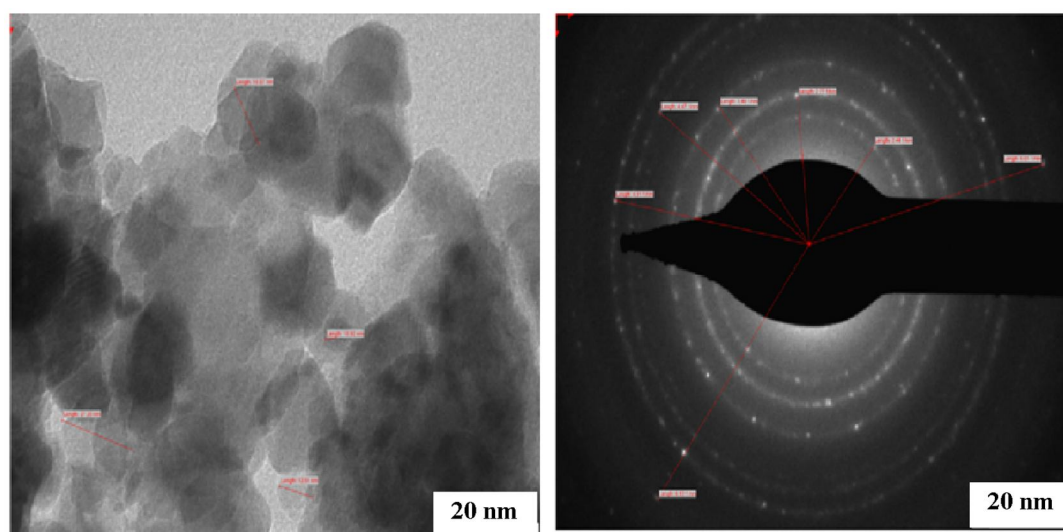


FIG. 3. (a) TEM image of $\text{Ni}_{0.5}\text{Co}_{0.5}\text{Al}_{0.5}\text{Fe}_{1.5}\text{O}_4$. FIG. (b) SAED image of $\text{Ni}_{0.5}\text{Co}_{0.5}\text{Al}_{0.5}\text{Fe}_{1.5}\text{O}_4$

Electric Resistivity

Fig. 4 shows the variation of electric resistivity with temperature for undoped and doped nickel-cobalt ferrites. From the figure, it is observed that electrical resistivity decreases exponentially with temperature, exhibiting semiconductor behavior. Similar behavior of electrical resistivity with temperature was reported by A. M. Bhavikattiet *al.* [19]. This decrease in electrical resistivity or increase in conductivity can be explained by Verwey's hopping mechanism.

According to Verwey [20], the conduction in ferrite is because of the exchange or hopping of electrons between ions of the same element with different valence states. In the present nickel-cobalt ferrites, conduction is due to simultaneous presence of ferrous (Fe^{2+}) and ferric (Fe^{3+}) ions on equivalent crystallographic sites usually the octahedral (B) sites and when electrons exchange from ferrous (Fe^{2+}) to ferric (Fe^{3+}) ions, conduction takes place. The extra electron which is present on a ferrous ion (Fe^{2+}) requires very small energy for exchange to ferric (Fe^{3+})

ion. With increase in temperature, charge carriers gain thermal energy, resulting in the increase in hopping rate and hence these extra electrons can be considered to be responsible for the increase in conductivity or decrease in resistivity.

From Fig. 4, it is also clear that resistivity increases with the addition of dopant Al^{3+} . The addition of aluminium in nickel-cobalt ferrite replaces the equal number of Fe^{3+} ions from the octahedral B-sites. The decrease in number of Fe^{3+} ions in octahedral sites results in the decrease of $\text{Fe}^{2+}/\text{Fe}^{3+}$ pairs contributing to the conduction which hinders the electron hopping

between Fe^{3+} and Fe^{2+} ions and consequently increases the resistivity with the addition of aluminium. Similar type of behavior in resistivity with Al^{3+} was reported by Le-Zhong Li [21]. As reported in the literature [22], resistivity of nanoparticles is dependent on the grain size and increases with decrease in grain size. Thus, in the present study, as the grain size decreases with addition of aluminium, the increase in resistivity is observed. Similar variation in electrical resistivity with Zn^{2+} doping in cobalt ferrite [5] and Al^{3+} in nickel ferrite is observed [23].

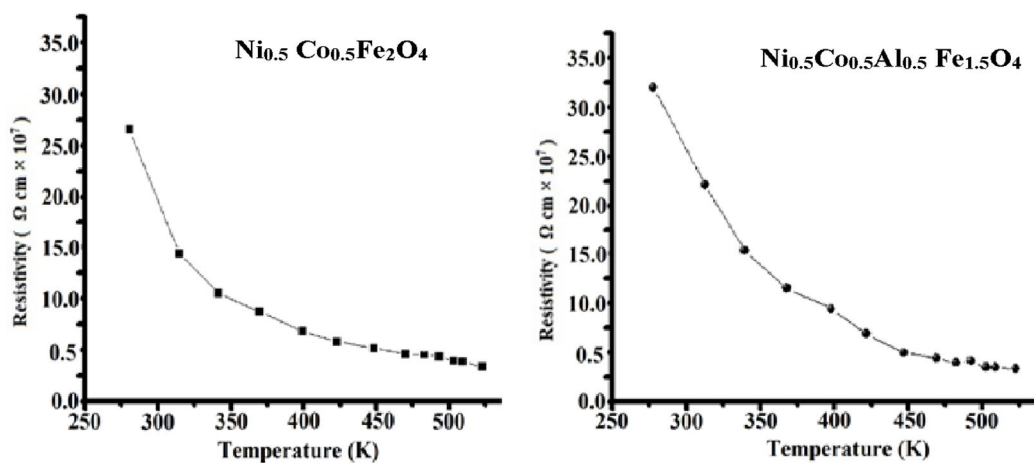


FIG. 4. Variation of electrical resistivity with temperature.

Dielectric Constant

Fig.5 shows the variation of dielectric constant with temperature at 100 Hz for undoped and doped nickel-cobalt ferrite. The figure shows that the dielectric constant increases steadily with increasing temperature up to the certain point of temperature, which is called the dielectric transition temperature (T_d). However, beyond this transition temperature, the dielectric constant is found to decrease. Similar variation of dielectric constant with temperature was observed by G. Sathish Kumar *et al.* [14] and G. R. Mohan *et al.* [24].

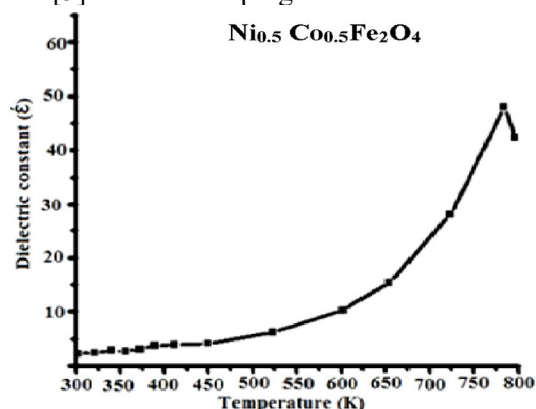
The variation of dielectric constant with temperature can be explained on the basis of hopping mechanism which is similar to that of mechanism of dielectric polarization. The electronic exchange between Fe^{2+} and Fe^{3+} in octahedral sites results in local displacements determining the polarization of charges in these ferrites.

With increase in temperature, charge carriers gain thermal energy and hopping of electrons is

thermally activated, resulting in an increase in polarization and thus dielectric constant increases. But, with further increase in temperature beyond dielectric transition temperature, charge carriers are less oriented towards the direction of the applied field and thus decrease the dielectric constant as reported by G. Sathish Kumar *et al.* [14] and G. R. Mohan *et al.* [24].

It can be understood from Fig. 5 that the dielectric constant decreases with the addition of aluminium in nickel-cobalt ferrite. The addition of Al^{3+} replaces the Fe^{3+} ions from the octahedral sites. Therefore, there will be a decrease in number of Fe^{3+} ions at B-site which plays a dominant role in dielectric polarization. Thus, electron exchange between Fe^{2+} and Fe^{3+} ions will be obstructed i.e., polarization will also decrease. As a result, dielectric constant decreases with addition of dopant aluminium. Similar behavior was observed by B. Vara Prasad for indium-substituted Ni-Zn ferrite system [25]. Similar type of behavior in dielectric constant with Zn^{2+} doping in cobalt

ferrite [5] and Al^{3+} doping in nickel ferrite was



observed [23].

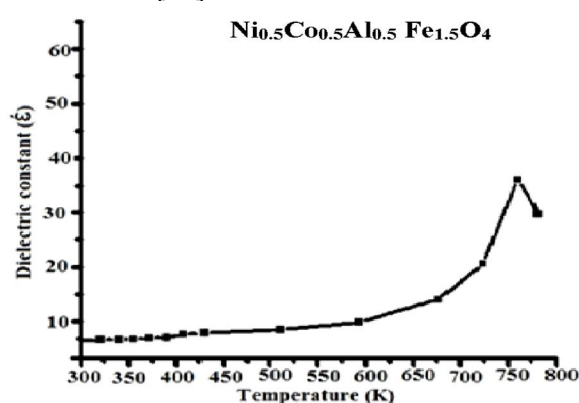


FIG. 5. Variation of dielectric constant with temperature.

Conclusion

$\text{Ni}_{0.5}\text{Co}_{0.5}\text{Al}_x\text{Fe}_{2-x}\text{O}_4$ ($x = 0$ and $x = 0.5$) nanoparticles have been effectively and successfully synthesized by microwave-assisted sol-gel auto-combustion method. The XRD analysis confirms single-phase cubic spinel structure with space group $\text{Fd}\bar{3}\text{m}$. Lattice parameter, particle size and X-ray density decrease, whereas porosity increases with Al substitution. EDX spectra confirmed the compositional formation of synthesized samples.

TEM confirmed the formation of nanocrystalline nature with single-phase spinel structure. Decreasing electrical resistivity with

temperature shows semiconducting nature. The dielectric constant increases with temperature and afterward decreases, which is due to the fact that electronic exchange between Fe^{2+} and Fe^{3+} and does not follow the direction of the applied field.

Acknowledgment

The authors acknowledge the Department of Nanoscience and Nanotechnology and the Department of Physics, Dr. Ambedkar College, Deekshabhoomi, Nagpur, for providing facilities and support to carry out this work.

References

- [1] Dabagh S., Ati A., Ghoshal S. K., Zare S., Roshan R. M., Jbara A. and Othaman Z., *Bull. Mater. Sci.*, 39(2016) 1029.
- [2] Patil R. P., Delekar S. D., Mane D. R. and Hankare P. P., *Results in Physics*, 3 (2013)129.
- [3] Lakshmi M., Kumar K. V. and Thyagarajan K., *Advances in Nanoparticles*, 5 (2016)103.
- [4] Khan S. B., Irfan S. and Long Lee S., *Nanomaterials*, 9 (1024) (2019) 1.
- [5] Bayoumi W., *J. Mater. Sci.*, 42 (2007)8254.
- [6] Kumar K. V., Paramesh D. and Reddy P. V., *World Journal of Nano Science and Engineering*, 5 (2015)68.
- [7] Singh H. S., Sangwa N. and Chauhan R., *International Journal of Scientific and Engineering Research*, 6 (12)(2015)765.
- [8] Venkatesha M., Kumara G. S., Vijia S., Karthib S. and Girijab E. K., *Modern Electronic Materials*, 2 (2016)74.
- [9] Cullity B. D., "Elements of X-ray Diffraction", 2nd edition, (Addison-Wesley Publishing Company, 1978).
- [10] Denton A. R. and Ashcroft N.W., *Vedard's Law, Physics Review, A* 43 (1991)3161.
- [11] Birajdar A. A., Shirsath S. E., Kadam R. H., Mane M. L. and Shitre A. R., *Journal of Applied Physics*, 112 (2012)053908.
- [12] Ladgaonkar B. P. and Vaigainkar A. S., *Materials Chemistry and Physics*, 56 (3)(1998)280.
- [13] Narasimhan C. S. and Swamy C. S., *Physica Status Solidi (a)*, 59 (1998)817.
- [14] Sathish Kumar G., Venkataraju C. and Sivakumar K., *Materials Sciences and Applications*, 1(2010) 19.

- [15] Amirabadizadeh A. and Amirabadi T., World Journal of Condensed Matter Physics, 3 (2013)131.
- [16] Arvind G. and Aranind D., Int. Journal of Engineering Research and Applications, 3 (6)(2013)1414.
- [17] Paramesh D., Kumar K. V. and Reddy P. V., Processing and Applications of Ceramics, 10 (3)(2016)161.
- [18] Lakshmi M., Kumar K. V. and Thyagarajan K., Journal of Nanostructure Chemistry, 5 (2015)365.
- [19] Bhavikatti A. M. and Mugli M., Proceedings of NCRIET-2015 & Indian Journal Science Research, 12 (1)(2015)232.
- [20] Verwey E. J. W., Haayman P. W. and Romeijn C.W., J. Chem. Phys.,15 (1947)181.
- [21] Li L.-Z., Zhong X.-X., Wang R., Tu X.-Q., He L., Guob, R. D. and Xu,Z.-Y., RSC Advances, 7 (2017)39198.
- [22] Wang Y. Z., Qiao G. W., Liu X.D., Ding B. Z. and Hu, Z. Q., Mater. Lett., 17(1993)152.
- [23] Waghmare S. P., Kakde A. S., Sisyawar A. C., Borikar D. M. and Rewatkar K. G., International Journal of Researchers in Bioscience, Agricultural & Technology, Special Issue (2) (2015) 2347.
- [24] Mohan G. R., Ravinder D., Ramana Reddy A. V. and Boyanov B. S., Materials Letters, 40 (1999)39.
- [25] Vara Prasad B. B.V. S., J. Theor. Appl. Phys., 9 (2015)267.